IUST
Iran University of Science and Technology

Iranian Journal of Electrical and Electronic Engineering

Journal Homepage: ijeee.iust.ac.ir

Research Paper

Sliding Mode Controller Design for Stabilization of the Three-Phase Grid-Connected Inverters in the Presence of Unbalanced Local Loads

A. Zakipour*(C.A.), K. Aminzare**, and M. Salimi***

Abstract: Considering the presence of different model parameters and controlling variables, as well as the nonlinear nature of DC to AC inverters; stabilizing the closed-loop system for grid current balancing is a challenging task. To cope with these issues, a novel sliding mode controller is proposed for the current balancing of local loads using grid-connected inverters in this paper. The closed-loop system includes two different controlling loops: a current controller which regulates the output current of grid-connected inverter and a voltage controller which is responsible for DC link voltage regulation. The main features of the proposed nonlinear controller are reactive power compensation, harmonic filtering and three-phase balancing of local nonlinear loads. The developed controller is designed based on the state-space averaged modelling its stability and robustness are proved analytically using the Lyapunov stability theorem. The accuracy and effectiveness of proposed controlled approach are investigated through the PC-based simulations in MATLAB/Simulink.

Keywords: Harmonic and Reactive Compensation, Robustness and Stability, Shunt Active Power Filter, Sliding Mode Control, Three-Phase Current Balancing, Wide Operational Range.

1 Introduction

IN recent years, the application of grid-connected voltage source inverters has found numerous applications in distributed generators, reactive power static compensators, energy storage systems, renewable energies, and shunt active power filters (SAPF) [1-3]. Conventionally, grid-connected voltage source inverters are stabilized using two-loop controllers. In such an approach, the inner loop is responsible for the regulation of inverter output current and can be implemented using either a hysteresis controller or linear methods. These closed-loop controlling approaches have been studied in recent years and their practical implementation is completely straightforward. Also, the industrial application of linear controllers in grid-connected inverters has been widely reported [4, 5]. To accomplish a linear controller design, the closed-loop system should be modelled using either an appropriate transform function or a state-space model. Considering the nonlinearity of converter, the system should be linearized around the operating point in both techniques [6]. If the operational range of a closed-loop system is wide, the stability of linear controller cannot be guaranteed since the small-signal approximation isn't valid anymore.

As another example, by using hybrid active power filters, a linear controller is developed for voltage ripple reduction at the point of common coupling as well as the load current compensating in [7]. The developed approach can cope with the malfunction and failure of

Iranian Journal of Electrical and Electronic Engineering, 2022.
Paper first received 08 March 2021, revised 13 June 2022, and accepted 29 June 2022.
* The author is with the Faculty of Electrical Engineering, Arak University of Technology (AUT), Arak, Iran.
E-mail: zakipour@arakut.ac.ir.
** The author is with the Islamic Azad University, Science and Research Branch, Tehran, Iran.
E-mail: kuroush@gmail.com.
*** The author is with the Faculty of Engineering and Science, University of Greenwich, Kent, UK.
E-mail: m.salimi@gre.ac.uk.
Corresponding Author: A. Zakipour.
https://doi.org/10.22068/IJEEE.18.3.2125

equipment and systems via power quality improvements. The linear controller is analyzed using the closed-loop transfer functions in both Laplace and discrete domains. However as mentioned before, a linear controller cannot guarantee the stability and robustness of controller in a wide range.

To cope with this issue, the application of adaptive linear controller has been reported in the literature which employs a range of PI gains for different operating points. Hence, the stability and performance of linear controllers can be improved in a wide range of operations [8, 9]. It should be noted that the swapping process between the different controllers imposes extra dynamics on the closed-loop system and can deteriorate the advantages of adaptive tuning.

Regarding the nature of grid-connected inverters, the application of modern nonlinear controllers has been reported in recent years [10-12]. The major nonlinear controllers are feedback linearization, passivity-based, sliding mode, and backstepping methods. In [13, 14], by defining a new state-vector, a mathematical and precise method is proposed to linearize (non-approximate) the input/output characteristic of closed-loop system (VSI inverter in grid-connected wind power plant) which is known as the exact-feedback linearization approach. In addition to injecting the generated wind power into the grid in the reference [13], the designed controller can track the maximum power point of generator. In [15], the application of passivity-based control method in grid-connected inverters has been studied for wind and photovoltaic power plants. However, in the mentioned nonlinear approaches in [10-15], uncertainty and robustness analysis of closed-loop system is not studied comprehensively.

The backstepping control method has been introduced by P. V. Kokotovic, and it is reported widely for closed-loop control of power electronics converters [11, 12, 16, 17]. The backstepping controller is more advantageous when it is combined with adaptive methods. However, it is well-known that the implementation of controller is a time-consuming task due to real-time adaptation rules which are essential for the estimation of uncertain parameters. So, the industrial application of backstepping controller is limited. On the other hand, a major feature of sliding mode nonlinear controllers is the ease of implementation. In the sliding mode controller (SMC), a sliding surface should be defined at first which can be a linear/nonlinear combination of error variables. The switching signals of converter are identified based on real-time location of state variables around the sliding surface.

In [18], the SMC is used to improve the total harmonic distortion (THD) of single-phase grid-connected voltage source inverter. A similar study has been performed in [19] to develop an SMC for a single-phase grid-connected inverter. In reference [19], the application of different hysteresis bands is essential for the generation of switching signals. However, the hysteresis control method results in variable switching frequency which complicates the EMI filter design as well as increases the coupling inductor size. In reference [20], the SMC is used to control the grid-connected wind energy conversion system. In the reference [21], the SMC is developed for a z-source converter and the equivalent control method is used to stabilize the switching frequency.

In [22], the SMC is designed for SAPF with LCL coupling to remove the distortive switching components properly. To cope with the phase shift issues in LCL coupling which is seen between the reference and injected currents and severely deteriorates the overall functionality of system, an SMC is developed for closed-loop stabilization. By using a modified signum function as well as an artificial increase of input-output relative degrees, it is tried to improve SMC response. However, the stability and robustness of developed SMC are not presented in [22], while an LCL coupling network can result in controller oscillation and instability issues.

The combination of sliding mode, adaptive backstepping, and fuzzy neural-network controllers is proposed for performance improvement of SAPF in [23]. The fuzzy neural network component is responsible for the approximation of nonlinear terms in the APF model and the removal of chattering in conventional SMCs. However, in addition to the complexity of controller real-time calculation in the adaptive methods, sufficient and appropriate data is required during the learning process of neural networks which can result in more challenges. Similar issues are seen in reference [24] which employs the radical bias function neural network with a complementary sliding mode method in SAPF.

In [25], the application of SMC is extended to the multi-level flying capacitor grid-connected inverters. Considering the features of multi-level converters, the current THD is decreased from 26.61% on the load side to 1.34% on the grid side. Despite the conventional SMCs, the control law is applied through the phase-shifted PWM unit to the switches and hence, the switching frequency of converter can be kept constant. As a result, small filters can be used grid connection of the inverter.

In addition to reactive power compensation and harmonic filtering of the local loads, grid connect inverters can be employed for grid current balancing in the three-phase systems. Due to the widespread application of single-phase loads in distribution networks, the presence of three-phase unbalanced currents is a common characteristic of distribution lines and transformers. In the active power filters, as the output currents of different phases can be adjusted independently, it is possible to mitigate this problem by defining a suitable reference current. However, the developed current controller should be fast and robust enough to track the references satisfactorily. So, in this

paper, the idea of using the SMC for source current balancing is proposed. According to our search and try, there is not any reported paper that applies the SMC for load current balancing in the active power filters. It should be noted that the SMC is a good choice for disturbance rejection as well. Moreover, if a precise model is employed for the controller design, better stability and robustness can be achieved against uncertain parameters. Hence in this article, the accuracy of averaged state-space model is improved by considering the parasitic elements. In this paper, a novel SMC is proposed for comprehensive compensation of nonlinear local loads, using the exact model of the system.

2 Averaged State-Space Model

The power circuit and simplified model of shunt active power filter (SAPF) have been shown in Figs. 1(a) and 1(b) respectively. By assuming xT = $[i_{fa}\ i_{fb}\ i_{fc}\ v_c]^T$ as state variables, the state-space model of the SAPF can be extracted as:

$$\frac{d}{dt}\begin{bmatrix} i_{fa} \\ i_{fb} \\ i_{fc} \\ v_C \end{bmatrix} = \begin{bmatrix} -\frac{R}{L} & 0 & 0 & \frac{1}{2L}u_a \\ 0 & -\frac{R}{L} & 0 & \frac{1}{2L}u_b \\ 0 & 0 & -\frac{R}{L} & \frac{1}{2L}u_c \\ -\frac{1}{2C}u_a & -\frac{1}{2C}u_b & -\frac{1}{2C}u_c & 0 \end{bmatrix} \begin{bmatrix} i_{fa} \\ i_{fb} \\ i_{fc} \\ v_C \end{bmatrix} + \begin{bmatrix} -\frac{1}{L}V_{aN} \\ -\frac{1}{L}V_{bN} \\ -\frac{1}{L}V_{cN} \\ 0 \end{bmatrix} \quad (1)$$

where $u_{a,b,c}$, $V_{aN,bN,cN}$, L, R, and C are averaged controller signals in switching frequency, PCC (point of common coupling) voltages, coupling inductance, the series equivalent resistance of coupling inductance and DC link capacitor respectively.

Considering instantaneous power theory, the dc side power in *dq0* synchronous reference frame can be written as:

$$V_c i_{dc} = \frac{3}{2}\left(e_{fd} i_{fd} + e_{fq} i_{fq} + 2e_{f0} i_{f0}\right) \quad (2)$$

where $e_{fq} = 0.5V_c u_q$, $e_{fd} = 0.5V_c u_d$, and $e_{f0} = 0.5V_c u_0$ are inverter output voltages in the *dq*0 reference frame respectively. Eq. (2) is used for i_{dc} calculation as:

$$i_{dc} = 3\left(u_d i_{fd} + u_q i_{fq} + 2u_0 i_{f0}\right) \quad (3)$$

By using (3), Eq. (1) can be simplified in *dq*0 synchronous reference frame as follows.

$$\frac{di_{fq}}{dt} = \left(-\frac{R}{L} i_{fq} - \omega i_{fd} - \frac{1}{L} v_{sq}\right) + \left(\frac{V_C}{2L} u_q\right) \quad (4)$$

$$\frac{di_{fd}}{dt} = \left(\omega i_{fq} - \frac{R}{L} i_{fd} - \frac{1}{L} v_{sd}\right) + \left(\frac{V_C}{2L} u_d\right) \quad (5)$$

$$\frac{di_{f0}}{dt} = \left(-\frac{R}{L} i_{f0} - \frac{1}{L} v_{s0}\right) + \left(\frac{V_C}{2L} u_0\right) \quad (6)$$

$$\frac{dV_c}{dt} = -\frac{3}{C}\left(u_d i_{fd} + u_q i_{fq} + 2u_0 i_{f0}\right) \quad (7)$$

where ω, $i_{fd,fq,f0}$, and $v_{sd,sq,s0}$ are rotating reference frame frequency, inverter currents and PCC voltages in the *dq0* reference frame.

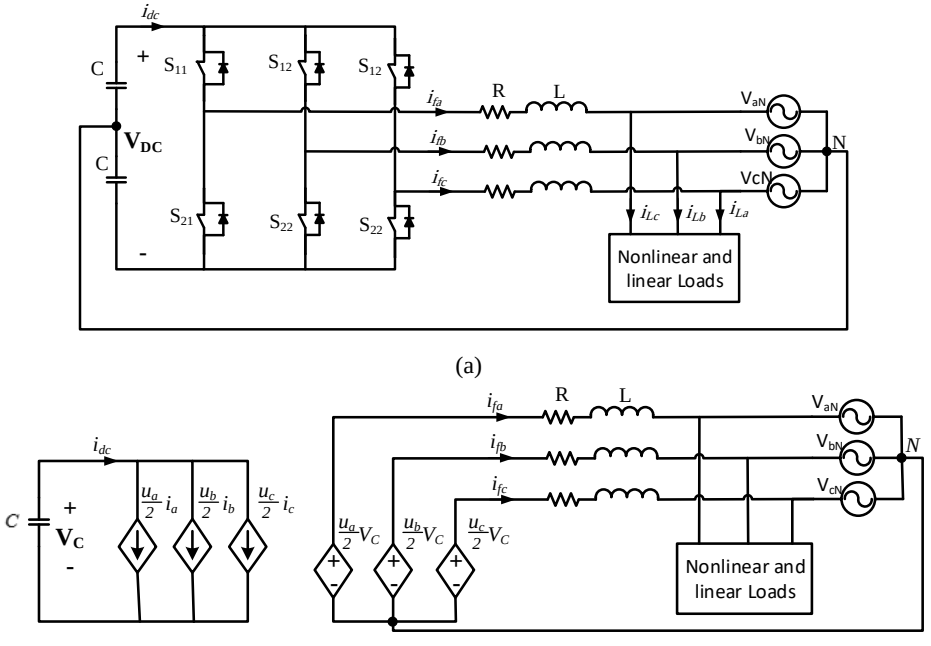

Fig. 1 Power circuit and simplified model of grid-connected SAPF; a) Power topology of the SAPF and b) Equivalent model of current-controlled voltage source inverter as a shunt active power filter.

3 Controller Design

3.1 Current Reference

The reference currents of SAPF can be obtained using the instantaneous power theory. In this method, the SAPF generates all reactive and harmonics components of load currents and only active parts of load currents are provided through the grid. Therefore, considering the synchronous rotating reference frame around the grid voltage, the variable V_{sq} can be assumed zero and then the active and reactive powers can be written as:

$$p = \bar{p} + \tilde{p} = \frac{3}{2}(V_{sd} i_{Ld} + 2V_{s0} i_{L0}) \tag{8}$$

$$q = \bar{q} + \tilde{q} = \frac{3}{2}\left(V_{sd} i_{Lq} + 2V_{s0} i_{L0}\right) \tag{9}$$

where $\bar{p}$, $\tilde{p}$, $\bar{q}$, $\tilde{q}$, i_{Ld}, i_{Lq}, and i_{L0} are averaged active power, distorted active power, averaged reactive power, distorted reactive power, and dq0 component of load currents respectively. Considering (8) and (9) and neglecting the PCC voltage variations, the block diagram of references current ($i_{fq}^* = i_{Lq}$, $i_{fd}^* = \bar{i}_{fd}^* + \tilde{i}_{fd}^*$, and $i_{f0}^* = i_{L0}$) generator is shown in Fig. 2. The active component of $\bar{i}_{Ld}$ can be defined using the capacitor voltage error:

$$\bar{i}_{fd}^* = k_p\left(V_c^* - V_c\right) + k_i \int \left(V_c^* - V_c\right) dt \tag{10}$$

3.2 MIMO-SMC Design

A nonlinear averaged state-space model of three-phase grid-connected SAPF is obtained in (4)-(7). According to the model, the parameters u_d, u_q, and u_0 are control inputs of SAPF. The variables i_d, i_q, and i_0 are system outputs that should be controlled. Also, dc side capacitor voltage should be indirectly regulated through the output currents. Hence, it is clear that the SAPF is a MIMO (multi-input multi-output) control system. Considering the internal link between the q and d axis, a closed-loop controller design which is based on the separation of variables and the use of two isolated controllers, cannot guarantee stability and robustness of the system. As a matter of fact, in three-phase SAPF, any variation in the control inputs will change all the system state variables. Hence, it is clear that stabilizing the MIMO SAPF with two separated SISO (single-input single-output) controllers cannot be a proper choice for a wide range of variations. To cope with this issue, in this paper, a MIMO-SMC is designed for three-phase SAPF.

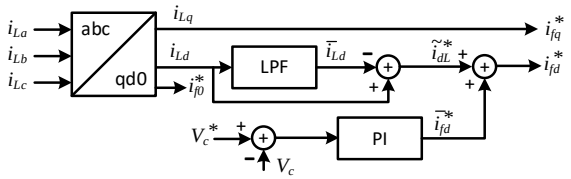

Fig. 2 Block diagram of reference currents generator.

In generic form, the averaged state-space model of system can be rewritten in the following format using (4)-(7):

$$\begin{aligned}\frac{di_{fq}}{dt} &= \dot{x}_1 \\ &= f_1\left(i_{fq}, i_{fd}, i_{f0}, V_C, t\right) + b_1\left(i_{fq}, i_{fd}, i_{f0}, V_C, t\right)u_q \\ &= \left(\hat{f}_1 + \tilde{f}_1\right) + \left(\hat{b}_1 + \tilde{b}_1\right)u_q\end{aligned} \tag{11}$$

$$\begin{aligned}\frac{di_{fd}}{dt} &= \dot{x}_2 \\ &= f_2\left(i_{fq}, i_{fd}, i_{f0}, V_C, t\right) + b_2\left(i_{fq}, i_{fd}, i_{f0}, V_C, t\right)u_d \\ &= \left(\hat{f}_2 + \tilde{f}_2\right) + \left(\hat{b}_2 + \tilde{b}_2\right)u_d\end{aligned} \tag{12}$$

$$\begin{aligned}\frac{di_{f0}}{dt} &= \dot{x}_3 \\ &= f_0\left(i_{fq}, i_{fd}, i_{f0}, V_C, t\right) + b_2\left(i_{fq}, i_{fd}, i_{f0}, V_C, t\right)u_d \\ &= \left(\hat{f}_3 + \tilde{f}_3\right) + \left(\hat{b}_3 + \tilde{b}_3\right)u_0\end{aligned} \tag{13}$$

$$\begin{aligned}\frac{dV_c}{dt} &= \dot{x}_4 \\ &= f_4\left(i_{fq}, i_{fd}, i_{f0}, V_C, t\right) + b_{41}\left(i_{fq}, i_{fd}, i_{f0}, V_C, t\right)u_q \\ &\quad + b_{42}\left(i_{fq}, i_{fd}, i_{f0}, V_C, t\right)u_d + b_{43}\left(i_{fq}, i_{fd}, i_{f0}, V_C, t\right)u_0 \\ &= \left(\hat{f}_3 + \tilde{f}_3\right) + \left(\hat{b}_{41} + \tilde{b}_{41}\right)u_q + \left(\hat{b}_{42} + \tilde{b}_{42}\right)u_d + \left(\hat{b}_{43} + \tilde{b}_{43}\right)u_0\end{aligned} \tag{14}$$

where $\hat{f}$, $\hat{b}$, $\tilde{f}$, and $\tilde{b}$ are nominal values and model uncertainties of f and b.

The reference values of output currents are defined in Section 3.1. The hyper-plane sliding surfaces are selected according to the AC-side current reference. Such an assumption can remove the steady-state error due to the application of integral terms.

$$\boldsymbol{S} = \left(\boldsymbol{X}_{1,2,3}^* - \boldsymbol{X}_{1,2,3}\right) + \boldsymbol{\alpha}\int\left(\boldsymbol{X}_{1,2,3}^* - \boldsymbol{X}_{1,2,3}\right)dt \tag{15}$$

or

$$\boldsymbol{S} = \begin{bmatrix} S_1 \\ S_2 \\ S_3 \end{bmatrix} = \begin{bmatrix} i_{fq}^* \\ i_{fd}^* \\ i_{f0}^* \end{bmatrix} - \begin{bmatrix} i_{fq} \\ i_{fd} \\ i_{f0} \end{bmatrix} + \begin{bmatrix} \alpha_1 & 0 & 0 \\ 0 & \alpha_2 & 0 \\ 0 & 0 & \alpha_3 \end{bmatrix} \begin{bmatrix} \int\left(i_{fq}^* - i_{fq}\right)dt \\ \int\left(i_{fd}^* - i_{fd}\right)dt \\ \int\left(i_{f0}^* - i_{f0}\right)dt \end{bmatrix} \tag{16}$$

or

$$S = \begin{bmatrix} S_1 \\ S_2 \\ S_3 \end{bmatrix} = \left(\boldsymbol{X}_{1,2,3}^* - \boldsymbol{X}_{1,2,3}\right) + \boldsymbol{\alpha} X_I$$

where S_1, S_2, and S_3 are sliding surfaces. Also, α_1, α_2,

and α_3 are positive design constant.

$$U = \bar{U} + \tilde{U} = \begin{bmatrix} u_q \\ u_d \\ u_0 \end{bmatrix} = \begin{bmatrix} \bar{u}_q + \tilde{u}_q \\ \bar{u}_d + \tilde{u}_d \\ \bar{u}_0 + \tilde{u}_0 \end{bmatrix} \tag{17}$$

By using (16), the time-derivative of the sliding surface can be written as:

$$\begin{aligned} \dot{\boldsymbol{S}} &= \left(\boldsymbol{X}^*_{1,2,3} - \boldsymbol{X}_{1,2,3}\right) + \boldsymbol{\alpha} X_I \\ &= \left(\dot{\boldsymbol{X}}^*_{1,2,3} - \left(\hat{\boldsymbol{F}}_{1,2,3} + \hat{\boldsymbol{B}}_{1,2,3}\bar{\boldsymbol{U}}\right)\right) + \alpha\left(\boldsymbol{X}^*_{1,2,3} - \boldsymbol{X}_{1,2,3}\right) \\ &= 0 \end{aligned} \tag{18}$$

To calculate the equivalent component of controller, derivatives of the sliding surfaces in (18) are set to zero considering the nominal values of the model parameters.

$$\bar{\boldsymbol{U}} = \hat{\boldsymbol{B}}^{-1}_{1,2,3}\left(\boldsymbol{\alpha}\left(\boldsymbol{X}^*_{1,2,3} - \boldsymbol{X}_{1,2,3}\right) + \dot{\boldsymbol{X}}^*_{1,2,3} - \hat{\boldsymbol{F}}_{1,2,3}\right) \tag{19}$$

By substituting the converter model in (19) and ignoring the equivalent series resistance of the inductors, the SMC controller can be obtained.

$$\bar{u}_q = \frac{2\left(v_{sq} + L\dfrac{di^*_{fq}}{dt} + Ri_{fq} + L\alpha_1\left(i^*_{fq} - i_{fq}\right) + L\omega i_{fd}\right)}{V_c} \tag{20}$$

$$\begin{aligned} \bar{u}_d = &\left[V_C\left(cV_C - 6Li_{fd}k_p\right)\right]^{-1} \times \\ &\Bigg[2\Bigg(cV_C v_{sd} - cLV_C^2 k_i + 12L^2 k_p V_C \frac{di^*_{f0}}{dt} + 6LRi^2_{fq}k_p \\ &+ 6L^2 i_{fq}k_p \frac{di^*_{fq}}{dt} - 6L^2\alpha_1 i^2_{fq}k_p + cRV_C i_{fd} \\ &+ 12LV_C k_p v_{s0} + 6Li_{fq}k_p v_{sq} + cLV_C V^*_c k_i \\ &- cLV_C\alpha_2 i_{fd} + cLV_C\frac{dV^*_c}{dt}k_p - cLV_C i_{fq}\omega \\ &+ 12LRV_C i_{f0}k_p - cLV^2_C\alpha_2 k_p - 12L^2V_C\alpha_3 i_{f0}k_p \\ &+ 12L^2V_C\alpha_3 i^*_{f0}k_p + 6L^2\alpha_1 i_{fq}i^*_{fq}k_p + 6L^2 i_{fd}i_{fq}k_p\omega \\ &+ cLV_C\alpha_2 k_i\int\left(V^*_c - V_c\right)dt + cL\alpha_2 k_p V_C V^*_c\Bigg)\Bigg] \end{aligned} \tag{21}$$

$$\bar{u}_0 = \frac{2\left(v_{s0} + L\dfrac{di^*_{f0}}{dt} + Ri_{f0} + L\alpha_3\left(i^*_{f0} - i_{f0}\right)\right)}{V_C} \tag{22}$$

The proposed MIMO-SMC includes two different components, equivalent ($\bar{u}_q, \bar{u}_d, \bar{u}_0$) and nonlinear ($\tilde{u}_q, \tilde{u}_d, \tilde{u}_0$) parts. The design process of mentioned controllers is described in the following. The nonlinear part of the MIMO-SMC is responsible for the improvement of system robustness and stability against load and grid voltage changes.

As it has been described previously, to improve the robustness of designed controllers against load and input voltage changes, model uncertainties and variations of the references in different operating points, the developed equivalent controller in (20)-(22) is combined with a nonlinear component.

Considering Eq. (19), the final SMC controller can be written as:

$$\begin{aligned} \boldsymbol{U} &= \bar{\boldsymbol{U}} + \boldsymbol{K}sgn\left(\boldsymbol{S}\right) \\ &= \hat{\boldsymbol{B}}^{-1}_{1,2,3}\left(\boldsymbol{\alpha}\left(\boldsymbol{X}^*_{1,2} - \boldsymbol{X}_{1,2}\right) + \dot{\boldsymbol{X}}^*_{1,2,3} - \hat{\boldsymbol{F}}_{1,2,3} + \boldsymbol{K}sgn\left(\boldsymbol{S}\right)\right) \end{aligned} \tag{23}$$

and the controller gain **K** is:

$$\boldsymbol{K} = \begin{bmatrix} k_1 & 0 & 0 \\ 0 & k_2 & 0 \\ 0 & 0 & k_3 \end{bmatrix} \tag{24}$$

According to (18), $\dot{S}$ can be simplified as:

$$\begin{aligned} \dot{\boldsymbol{S}} = \dot{\boldsymbol{X}}^*_{1,2,3} - \Big(&\boldsymbol{F}_{1,2,3} + \boldsymbol{B}_{1,2,3}\hat{\boldsymbol{B}}^{-1}_{1,2,3}\Big(\alpha\left(\boldsymbol{X}^*_{1,2,3} - \boldsymbol{X}_{1,2,3}\right) \\ &+ \dot{\boldsymbol{X}}^*_{1,2,3} - \hat{\boldsymbol{F}}_{1,2,3} + \boldsymbol{K}sgn\left(\boldsymbol{S}\right)\Big)\Big) + \boldsymbol{\alpha}\dot{\boldsymbol{X}}_I \end{aligned} \tag{25}$$

In (25), the parameter **B** can be defined as:

$$\begin{aligned} \boldsymbol{B}_{1,2,3} &= \hat{\boldsymbol{B}}_{1,2,3} + \tilde{\boldsymbol{B}}_{1,2,3} = \left(\boldsymbol{I} + \Delta\right)\hat{\boldsymbol{B}}_{1,2,3} \\ &\left|\Delta_{ij}\right| \le D_{ij} \quad i, j = 1,2,3 \end{aligned} \tag{26}$$

In (26), the matrix **I** is a 3×3 identity one, so it is clear that $\mathbf{B}\hat{\mathbf{B}}^{-1} = \left(\mathrm{I} + \Delta\right)$. Moreover, Δ is a 3×3 matrix and Δ_{ij} are its elements. On the other hand, it is obvious that $\Delta_{ij} = 0$ for $i \neq j$. So, the time-derivate of (25) can be simplified as:

$$\begin{aligned} \dot{\boldsymbol{S}} = &\boldsymbol{\alpha}\left(2\boldsymbol{I} + \Delta\right)\dot{\boldsymbol{X}}_I + \left(\hat{\boldsymbol{F}}_{1,2,3} - \boldsymbol{F}_{1,2,3}\right) \\ &- \left(\boldsymbol{I} + \Delta\right)\boldsymbol{K}sgn\left(\boldsymbol{S}\right) - \Delta\dot{\boldsymbol{X}}^*_{1,2} + \Delta\hat{\boldsymbol{F}}_{1,2,3} \end{aligned} \tag{27}$$

To investigate the stability and robustness of developed nonlinear controller, it is enough to evaluate the following criteria:

$$S_i\dot{S}_i \le -\eta_i\left|S_i\right| \qquad \left(\eta_i > 0\right) \tag{28}$$

In (28), η_i is a positive scalar. Considering (28), the mentioned condition can be rewritten as follows:

$$\begin{aligned} S_1\Big(\left(f_1 - \hat{f}_1\right) - k_1\left(1 + \Delta_{11}\right)sgn\left(S_1\right) + \Delta_{11}\left(\hat{f}_1 - \dot{x}^*_1\right) \\ + \left(2 + \Delta_{11}\right)\alpha_1\tilde{x}_1\Big) \le \left|S_1\right|\Big(\left|f_1 - \hat{f}_1\right| - \left(1 - D_{11}\right)k_1 \\ + D_{11}\left|\hat{f}_1 - \dot{x}^*_1\right| + \left(2 + D_{11}\right)\alpha_1\left|\tilde{x}_1\right|\Big) \le -\eta_1\left|S_1\right| \end{aligned} \tag{29}$$

If it is assumed that $\left|f_i - \hat{f}_i\right| \le f_{I,Max}$, then (29) can be written as:

$$f_{1,Max} + D_{11}\left|\hat{f}_1 - \dot{x}_1^*\right| + \left(2 + D_{11}\right)\alpha_1\left|\tilde{x}_1\right| + \eta_1 \le \left(1 - D_{11}\right)k_1 \quad (30)$$

For the second and third sliding surfaces, the condition can be obtained as:

$$f_{2,Max} + D_{22}\left|\hat{f}_2 - \dot{x}_2^*\right| + \left(2 + D_{22}\right)\alpha_2\left|\tilde{x}_2\right| + \eta_2 \le \left(1 - D_{22}\right)k_2 \quad (31)$$

$$f_{3,Max} + D_{33}\left|\hat{f}_3 - \dot{x}_3^*\right| + \left(2 + D_{33}\right)\alpha_3\left|\tilde{x}_3\right| + \eta_3 \le \left(1 - D_{33}\right)k_3 \quad (32)$$

Hence, if k_1, k_2, and k_3 can be selected as follows, the stability of developed SMC can be guaranteed:

$$k_1 \ge \left(1 - D_{11}\right)^{-1}\left(f_{1,Max} + D_{11}\left|\hat{f}_1 - \dot{x}_1^*\right| + \left(2 + D_{11}\right)\alpha_1\left|\tilde{x}_1\right| + \eta_1\right) \quad (33)$$

$$k_2 \ge \left(1 - D_{22}\right)^{-1}\left(f_{2,Max} + D_{22}\left|\hat{f}_2 - \dot{x}_2^*\right| + \left(2 + D_{22}\right)\alpha_2\left|\tilde{x}_2\right| + \eta_2\right) \quad (34)$$

$$k_3 \ge \left(1 - D_{33}\right)^{-1}\left(f_{3,Max} + D_{33}\left|\hat{f}_3 - \dot{x}_3^*\right| + \left(2 + D_{33}\right)\alpha_2\left|\tilde{x}_3\right| + \eta_3\right) \quad (35)$$

Finally, if the Lyapunov function is selected as $V(t) = 0.5S_1^2 + 0.5S_2^2 + 0.5S_3^2$, it can be seen that the time-derivative of Lyapunov function will be equal to $dV/dt \le -\eta_1|S_1| - \eta_2|S_2| - \eta_3|S_3|$ which is a negative semidefinite function and results in the stability and robustness of developed controller.

4 Simulation Results

To evaluate the response of proposed current controller for active power filters, it is simulated in MATLAB/Simulink toolbox. Simulation parameters are listed in Table. I. To study the response of system to unbalanced loads, three single-phase full-bridge diode rectifiers with RL load are employed as a nonlinear load of system. The values of DC load on the rectifier sides are equal to 100Ω, 25µH for phase A, 5Ω, 12µH for phase B and 15Ω, 33µH for phase C. So, it is clear that the three-phase load currents will be unbalanced in a steady-state condition. It should be noted that the switching frequency of converter is 20kHz in the simulation results.

4.1 Test 1: Steady-State Operation

In Fig. 3, the response of proposed nonlinear controller is investigated during steady-state operation. Despite considerable harmonics in load current, it is seen that the source current is completely sinusoidal and in phase with load voltage. Also, the proposed active power filter is capable of balancing the source current.

Table 1 Simulation parameters.

Parameter		Value	Unit
DC link voltage		800	V
Coupling inductance		500	µH
Resistance of the coupling impedance		0.1	Ω
Source voltage		220	V (rms)
Switches on resistance		0.1	ohm
Gains of the DC link voltage controller	k_p	0.5	-
	k_i	10	
Gains of the SMCs	α_1, α_2, and α_3	80	-
	k_1, k_2, and k_3	1	
Switching frequency	f_s	20	kHz

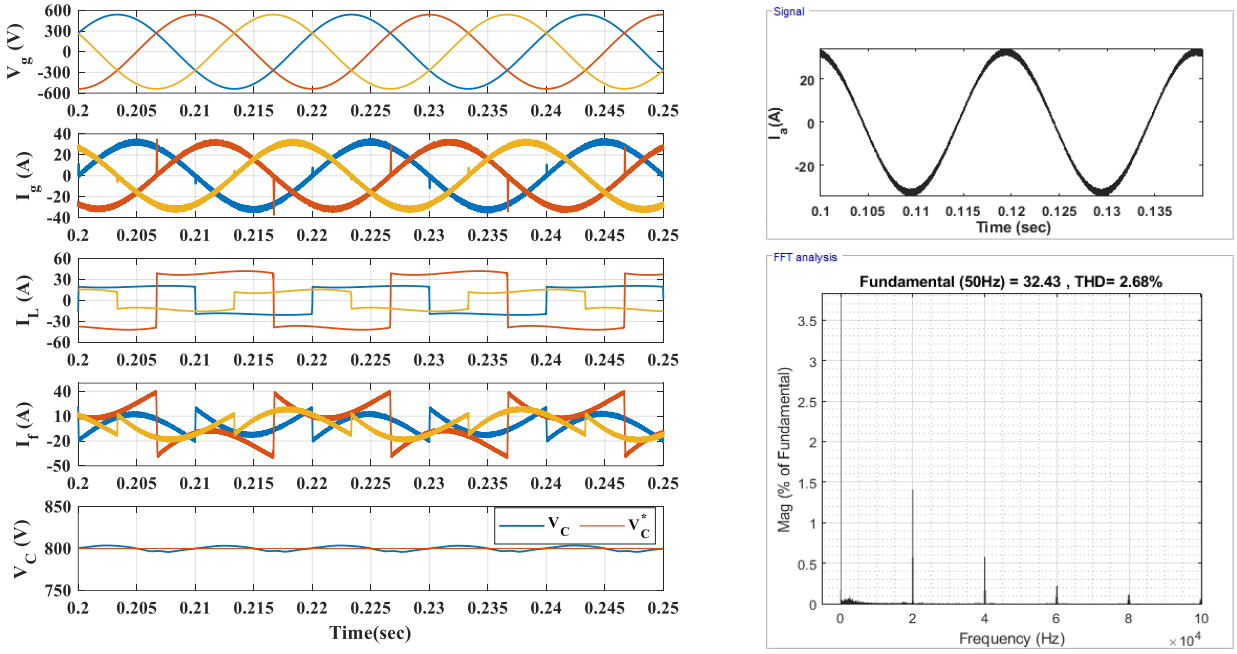

(a) (b)

Fig. 3 Steady-state operation of proposed control strategy as an active power filter; a) Grid voltage, grid, load and filter currents, and SC link voltage and b) Grid current THD.

This issue is completely vital for the optimal utilization of electric grids, including distribution lines and transformers. Despite the square waveform of load current, it is shown that the grid current THD is about 1.6% in Fig. 3(a), which is compatible with the IEE-IEC harmonic standards [26]. Regarding the comparison of proposed approach with existing works, the reference [27] which has been published in 2022 is selected for this purpose. Considering the general functionality of active power filters, the THD value of grid current is used as a comparison parameter. According to the simulation results, it is seen that the grid current THD is less than 2.68% in the proposed SMC. It should be noted that the THD value for reference [27] is more than 5%.

4.2 Test 2: Dynamic Response of the Proposed Current Controller

To study the dynamic response of proposed controller during load changes, it is assumed that the active power filter is not running at first. Then, at t = 0.04s it is started to compensate the load undesired components. In Fig. 4, the current and voltage of phase B are illustrated during system start-up. It is seen that after the operation of proposed closed-loop system, the source current will be completely sinusoidal and in phase with its voltage. Also, the dynamic response of the controller is fast and there is not any oscillation during transient moments.

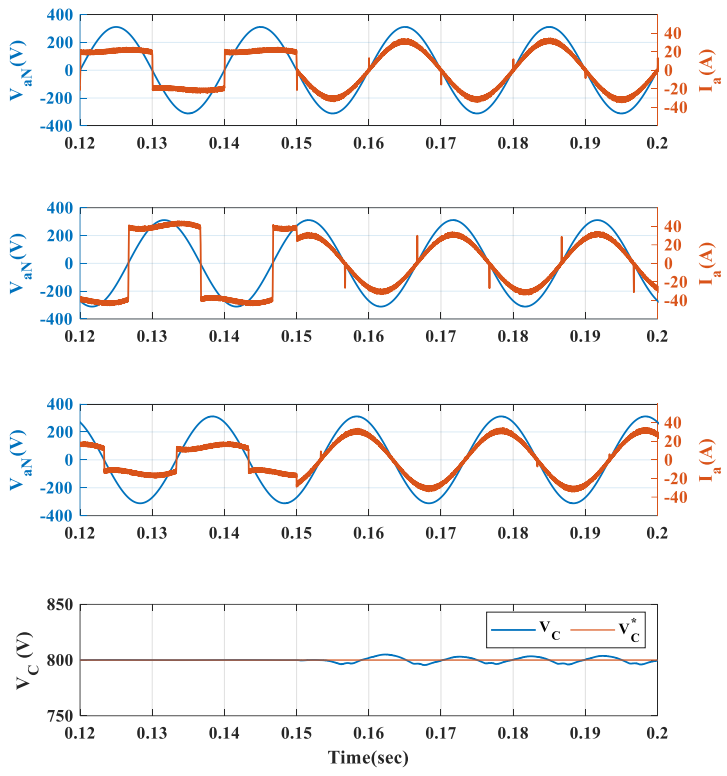

Fig. 4 Voltage and current for phase A of the utility before and after filter operation.

4.3 Test 3: Dynamic Response of the DC Link Voltage Controller

During the system start-up, the DC link voltage is zero and it is charged up to the reference value (800 V) by absorbing a defined active power from the utility. In Fig. 5, the dynamic response of the voltage controller is illustrated. It is seen that despite voltage changes in a very wide range from zero to nominal value, the capacitor is charged smoothly and there is not any overshoot. Also, the DC link voltage error is zero during steady-state operation.

4.4 Test 4: Dynamic Changes of the Reference Values

In Fig. 6, the response of the proposed controller to dynamic changes in the phase and amplitude of the reference values is shown. Variation of the current reference value, the output current of the inverter and its error is illustrated. Despite the reference values changes in a wide range of operations, it is observed that the developed controller is completely fast and robust with zero steady-state error.

5 Conclusion

In this paper, a novel nonlinear and robust controller is developed for three-phase SAPF using the SMC. Considering the existence of different controlling

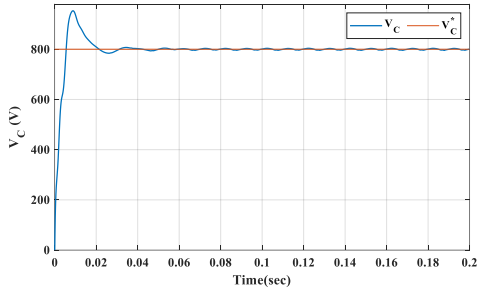

Fig. 5 DC link voltage changes during system start-up.

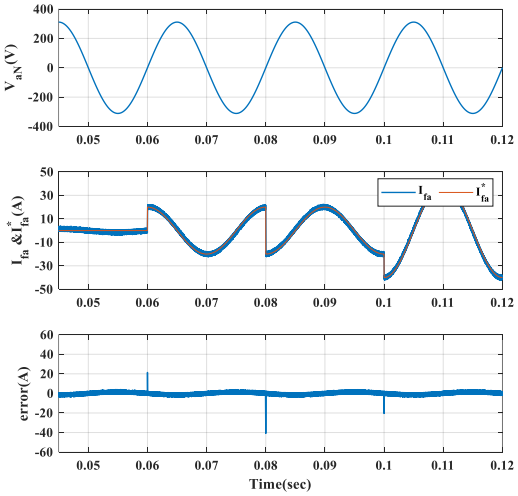

Fig. 6 Dynamic response of the proposed controller to step changes of the phase and amplitude of the reference value.

inputs/outputs in the averaged steady-state model of system, a unique controller is proposed for the stabilization of closed-loop system in a wide operational range. Considering the simulation results of designed controller in MATLAB/Simulink toolbox, the response of developed active power filter is investigated regarding the harmonic filtering and three-phase current balancing of local loads. It is seen that the proposed approach can compensate for the harmonic and reactive components of the local loads. Moreover, it can mitigate the unbalance component of grid current in three-phase systems. Finally, the current controller is fast enough to track the high-frequency reference signal and improve the power quality of utility with zero steady-state error. Although the load current is almost a square waveform, the developed controller can maintain the grid current around 2.68% which is in the IEEE/IEC harmonic standard ranges.

Funding

No funding was received for this work.

CRediT Authorship Contribution Statement

A. Zakipour: Idea & conceptualization, Research & investigation, Methodology, Project administration, Supervision, Verification, Revise & editing. **K. Aminzare:** Software and simulation, Data curation, Original draft preparation, Idea & conceptualization, Revise & editing. **M. Salimi:** Analysis, Revise & editing, Idea & conceptualization, Methodology.

Declaration of Competing Interest

The authors hereby confirm that the submitted manuscript is an original work and has not been published so far, is not under consideration for publication by any other journal and will not be submitted to any other journal until the decision will be made by this journal. All authors have approved the manuscript and agree with its submission to "Iranian Journal of Electrical and Electronic Engineering".

References

[1] X. Du, C. Zhao, and J. Xu, "The use of the hybrid active power filter in LCC-HVDC considering the delay-dependent stability," *IEEE Transactions on Power Delivery*, Vol. 37, No. 1, pp. 664–673, 2021.

[2] M. Guan, "Scheduled power control and autonomous energy control of grid-connected energy storage system (ESS) with virtual synchronous generator and primary frequency regulation capabilities," *IEEE Transactions on Power Systems*, Vol. 37, No. 2, pp. 942–954, 2021.

[3] M. A. Khan, A. Haque, V. B. Kurukuru, and M. Saad, "Advanced control strategy with voltage sag classification for single-phase grid-connected photovoltaic system," *IEEE Journal of Emerging and Selected Topics in Industrial Electronics*, Vol. 3, No. 2, pp. 258–269, 2020.

[4] X. Zhao and L. Chang, "Active and reactive power decoupling control of grid-connected inverters in stationary reference frame," *Chinese Journal of Electrical Engineering*, Vol. 3, No. 3, pp. 18–24, 2017.

[5] D. Pan, X. Ruan, C. Bao, W. Li, and X. Wang, "Capacitor-current-feedback active damping with reduced computation delay for improving robustness of LCL-type grid-connected inverter," *IEEE Transactions on Power Electronics*, Vol. 29, No. 7, pp. 3414–3427, 2013.

[6] X. Lin, J. Yu, R. Yu, J. Zhang, Z. Yan, and H. Wen, "Improving small-signal stability of grid-connected inverter under weak grid by decoupling phase-lock loop and grid impedance," *IEEE Transactions on Industrial Electronics*, Vol. 69, No. 7, pp. 7040–7053, 2022.

[7] S. Dehghan, V. A. Yazdian, and M. Mohammadian, "Hybrid series & shunt active DC line conditioner," *Iranian Journal of Electrical and Electronic Engineering*, Vol. 2, No. 2, pp. 47–56, 2006.

[8] M. Alizadeh and S. S. Kojori, "Augmenting effectiveness of control loops of a PMSG (permanent magnet synchronous generator) based wind energy conversion system by a virtually adaptive PI (proportional integral) controller," *Energy*, Vol. 91, pp. 610–629, 2015.

[9] D. Ton Duc, L. Viet Quoc, C. Young-Sik, C. Han Ho, and J. Jin-Woo, "An adaptive voltage control strategy of three-phase inverter for stand-alone distributed generation systems," *IEEE Transactions on Industrial Electronics*, Vol. 60, No. 12, pp. 5660–5672, 2013.

[10] H. Katir, A. Abouloifa, K. Noussi, I. Lachkar, A. E. Aroudi, M. Aourir, F. E. Otmani, and F. Giri, "Fault tolerant backstepping control for double-stage grid-connected photovoltaic systems using cascaded H-bridge multilevel inverters," *IEEE Control Systems Letters*, Vol. 6, pp. 1406–1411, 2022.

[11] N. N. Nam, N. D. Nguyen, C. Yoon, M. Choi, and Y. I. Lee, "Voltage sensorless model predictive control for a grid-connected inverter with *LCL* filter," *IEEE Transactions on Industrial Electronics*, Vol. 69, No.1, pp. 740–751, 2022.

[12] M. Salimi, J. Soltani, G. A. Markadeh, and N. R. Abjadi, "Indirect output voltage regulation of DC-DC buck/boost converter operating in continuous and discontinuous conduction modes using adaptive backstepping approach," *IET Power Electronics*, Vol. 6, No. 4, pp. 732–741, 2013.

[13] C. Jian, L. Jiang, Y. Wei, and Q. H. Wu, "A feedback linearization control strategy for maximum power point tracking of a PMSG based wind turbine," in *International Conference on Renewable Energy Research and Applications (ICRERA)*, pp. 79–84, 2013.

[14] B. Xianwen, Z. Fang, T. Yuan, and T. Peixuan, "Simplified feedback linearization control of three-phase photovoltaic inverter with an LCL filter," *IEEE Transactions on Power Electronics*, Vol. 28, pp. 2739–2752, 2013.

[15] J. Wang, X. Mu, and Q. K. Li, "Study of passivity-based decoupling control of T-NPC PV grid-connected inverter," *IEEE Transactions On Industrial Electronics*, Vol. 64, No. 9, pp. 7542–7551, 2017.

[16] M. Salimi, J. Soltani, and A. Zakipour, "Experimental design of the adaptive backstepping control technique for single-phase shunt active power filters," *IET Power Electronics*, Vol. 10, No. 8, pp. 911–918, 2017.

[17] W. Rong-Jong, L. Chih-Ying, W. Wen-Chuan, and H. Hsin-Ning, "Design of backstepping control for high-performance inverter with stand-alone and grid-connected power-supply modes," *IET Power Electronics*, Vol. 6, No. 4, pp. 752–762, 2013.

[18] H. Xiang, Y. Xu, L. Tao, H. Lang, and C. Wenjie, "A sliding-mode controller with multiresonant sliding surface for single-phase grid-connected VSI with an LCL filter," *IEEE Transactions on Power Electronics*, Vol. 28, No. 5, pp. 2259–2268, 2013.

[19] H. Komurcugil, S. Ozdemir, I. Sefa, N. Altin, and O. Kukrer, "Sliding-mode control for single-phase grid-connected LCL-filtered VSI with double-band hysteresis scheme," *IEEE Transactions on Industrial Electronics*, Vol. 63, pp. 864–873, 2016.

[20] Y. Errami, M. Ouassaid, M. Cherkaoui, and M. Maaroufi, "Sliding mode control scheme of variable speed wind energy conversion system based on the PMSG for utility network connection," in *Advances and Applications in Sliding Mode Control systems*, T. A. Azar and Q. Zhu, Eds., ed Cham: Springer International Publishing, pp. 167–200, 2015.

[21] A. Zakipour, S. Shokri Kojori, and M. Tavakoli Bina, "Closed-loop control of the grid-connected Z-source inverter using hyper-plane MIMO sliding mode," *IET Power Electronics*, Vol. 10, No. 15, pp. 2229–2241, 2017.

[22] M. A. E. Alali, Y. B. Shtessel, and J. Barbot, "Grid-connected shunt active *LCL* control via continuous sliding modes," *IEEE/ASME Transactions on Mechatronics*, Vol. 24, No. 2, pp. 729–740, 2019.

[23] Y. Fang, J. Fei, and T. Wang, "Adaptive backstepping fuzzy neural controller based on fuzzy sliding mode of active power filter," *IEEE Access*, Vol. 8, pp. 96027–96035, 2020.

[24] J. Fei, N. Liu, S. Hou, and Y. Fang, "Neural network complementary sliding mode current control of active power filter," *IEEE Access*, Vol. 9, pp. 25681–25690, 2021.

[25] A. Zakipour, N. Ghaffari, and M. Salimi, "State space modeling and sliding mode current control of the grid connected multi-level flying capacitor inverters," *Journal of Electrical and Computer Engineering Innovations (JECEI)*, Vol. 9, No. 2, pp. 215–228, 2021.

[26] S. M. Halpin, "Comparison of IEEE and IEC harmonic standards," in *IEEE Power Engineering Society General Meeting*, pp. 2214–2216, 2005.

[27] R. Kumar, H. O. Bansal, A. R. Gautam, O. P. Mahela, and B. Khan, "Experimental investigations on particle swarm optimization based control algorithm for shunt active power filter to enhance electric power quality," *IEEE Access*, Vol. 10, pp. 54878–54890, 2022.

A. Zakipour was born in Iran, in 1981. He received his Ph.D. degree in Electrical Engineering from the K. N. Toosi University of Technology, Tehran, Iran, in 2017. Currently, he is an Assistant Professor of Electrical Engineering, Power Electronics at the Department of Electrical Engineering, Arak university of Technology. His research interests include the design and control of the DC/DC and DC/AC converters, grid-connected inverters, and variable speed drives.

K. Aminzare received the B.Sc. degree in Electrical Engineering from the Islamic Azad University South Tehran Branch, Iran, in 2006 and the M.Sc. degree from Islamic Azad University Science and Research Branch, Iran in 2017. His research interests include nonlinear control of active power filters and grid-connected inverters.

M. Salimi graduated in Electrical Engineering from Islamic Azad University (IAU) (Science and Research Branch) Tehran, Iran in 2012. He worked as an Assistant Professor from 2012 until 2019 at the IAU University, Ardabil Branch, Iran, in the Electrical and Electronics Department. In 2019 he joined the University of Nottingham, Power Electronics, Machine, and Control (PEMC) group as a researcher for three years. Since April 2022, he has worked at Greenwich University as a lecturer of power electronics. He has published 31 papers in peer-reviewed journals with 24 papers published in international conferences. Areas of research include design, closed-loop control, simulation, and practical implementation of the power electronics systems for more/full electric aircraft and vehicles, grid-connected renewable energy systems, and active power filters.